Mon. Not. R. astr. Soc. (1991) **250**, 644–649

MERLIN and VLA observations of the quasar 1150 + 497

Chidi E. Akujor ★ and Simon T. Garrington
University of Manchester, Nuffield Radio Astronomy Laboratories, Jodrell Bank, Macclesfield SK11 9DL

Accepted 1991 February 1. Received 1991 January 31; in original form 1990 December 10

SUMMARY

We present new high-resolution MERLIN and VLA maps of the quasar 1150 + 497 which has a bright jet with compact knots and sharp bends, but no prominent hotspot. The source shows very little variation of Faraday rotation or depolarization. We discuss whether this is a disrupting jet which is intrinsically bright or whether it simply appears bright due to Doppler beaming.

1 INTRODUCTION

High-resolution observations using MERLIN and the VLA have revealed jets in the majority of radio-loud quasars, confirming the 'beam' model of Scheuer (1974) and Blandford & Rees (1974) whereby energy is transported by collimated beams to the outer radio lobes. Hydrodynamical simulations of such jets (Norman *et al.* 1982) have shown that light supersonic jets propagate stably through the surrounding intergalactic medium and end in a strong shock where electrons may be accelerated to relativistic energies producing the bright synchrotron emission seen as hotspots. Some quasars, however, such as 3C9 and 3C280.1 (Swarup, Sinha & Saikia 1982), 1857 + 566 (Saikia *et al.* 1983), and 0800 + 608 (Jackson *et al.* 1990) have bright jets which do not end in bright hotspots. It has been suggested that these jets lose a substantial part of their bulk kinetic energy through internal shocks or instabilities and hence cannot form bright hotspots.

The quasar 1150 + 497 (4C49.22), one of the first to show a bright one-sided jet (Perley 1981), is another example of a bright jet without a prominent hotspot. In this paper we present MERLIN and VLA observations at 408, 1465, 1515, 1665, 4885 and 14915 MHz with angular resolutions between 1 and 0.1 arcsec. We discuss the structure of the jet, its magnetic field configuration and the distributions of Faraday rotation and spectral index.

2 OBSERVATIONS

Table 1 gives details of the observations. The absolute flux scale was based on observations of 3C286 and 3C48 (Baars *et al.* 1977). The instrumental polarization of the VLA was calibrated by observations of point sources, and the polarization position angle scale was established by assuming a value of 33° for 3C286 between 1.4 and 5 GHz (Perley 1982). All the maps were made using the self-calibration algorithm (Cornwell & Wilkinson 1981), and the MERLIN maps were made with the OLAF MAP programme (see Davis, Muxlow & Conway 1985).

The maps presented below (Figs 1–4) reproduce accurately the main features of the jet but not the diffuse northern lobe or the surrounding halo. This is due to the lack of short interferometer spacings and residual calibration errors which appear as sidelobes around the core and jet. A low-resolution map made by tapering the 1665-MHz data to give more weight to the shorter baselines shows that the source does have a well-defined outer boundary and includes at least 80 per cent of the source flux density measured by a single dish (Kühr *et al.* 1981).

3 TOTAL INTENSITY STRUCTURE

As earlier maps have shown (Perley 1981; Linfield 1983; Owen & Puschell 1984), the source has an asymmetric triple structure with a diffuse northern lobe, a bright core and a bright one-sided jet. The low-resolution maps (Figs 1 and 2) show a diffuse halo surrounding the whole source. The northern lobe has a steep spectrum with $\alpha = 0.9$ (where $S \propto \nu^{-\alpha}$). This lobe contains no hotspot – any peak is less than twice the level of the 'plateau'. The appearance of the lobes suggests a filamentary structure, similar to that seen in the southern lobe of 0800 + 608 (Jackson *et al.* 1990), but

Table 1. Details of MERLIN and VLA observations of 1150 + 497.

Frequency MHz	Array	Date	Resolution arcseconds	Noise level mJy/beam
408	MERLIN	July 1981	1.0	0.12
1465	VLA-A	April 1986	1.0	0.21
1515	VLA-A	April 1986	1.0	0.23
1665	VLA-A	October 1985	1.0	0.03
1660	MERLIN	August 1980	1.0	0.43
4835	VLA-A	July 1986	0.35	0.09
4885	VLA-B	October 1985	1.0	0.16
4995	MERLIN	May 1982	0.15	0.16
14914	VLA-A	October 1895	0.1	0.27

★ Permanent address: Astrophysics Group, Department of Physics and Astronomy, University of Nigeria, Nsukka, Nigeria.

the details of this structure will require more sensitive observations.

At 5 GHz (Fig. 3) the core flux density is 338 mJy (~30 per cent of the total flux density). The core has a flat spectrum ($\alpha = 0.11$) between 1.6 and 15 GHz. The present maps, along with previously published maps, indicate a steady decline in the core flux density of about 50 per cent over the last seven years.

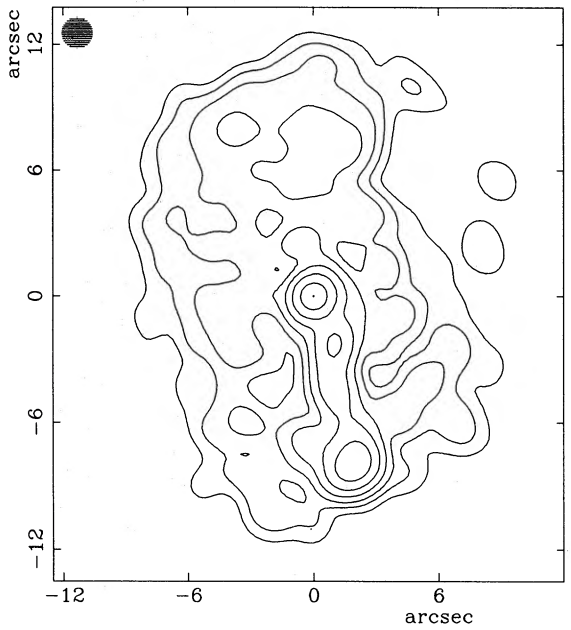

Figure 1. MERLIN 408-MHz map of 1150+497. The restoring beam is 1.0 arcsec and contours are drawn at 0.5, 1, 2,..., 50 and 99 per cent of the peak brightness which is 348 mJy beam^{-1}.

The structure of the jet is most clearly seen in the VLA 5-GHz map (Fig. 3). The first knot in the arcsec scale jet is in position angle $216 \pm 1.5°$ compared to the VLBI jet which emerges at $208 \pm 3°$ (Linfield 1983). The MERLIN 5-GHz map shows that the bend in the jet occurs just after the bright knot B. The appearance of the jet in the central region (features E, F and G) is similar to the jet of 0800+608 and the inner jet of M87 (Owen, Hardee & Cornwell 1989), with a straight outer edge and brighter features within the jet which are inclined to the direction of the jet. If the source has a hotspot, it is the southern-most compact knot visible in the MERLIN maps (Fig. 4a and 4b). While the surface brightness of the knot is high, about 31 mJy arcsec^{-2}, its total flux density is only 6 mJy, accounting for no more than 1 per cent of the source flux density. In our 15-GHz 'snap-shot' map (not shown), the bright knots in the jet are only marginally detected due to lack of surface brightness sensitivity. The spectral index measured between the VLA maps at 1.6 and 5 GHz is fairly constant along the jet ($\alpha \simeq 0.6$) and does not vary significantly at the bright knots.

4 POLARIZATION CHARACTERISTICS

The core is 2 per cent polarized at 5 GHz with the ***B***-vector parallel to the initial jet direction. This is typical for lobe-

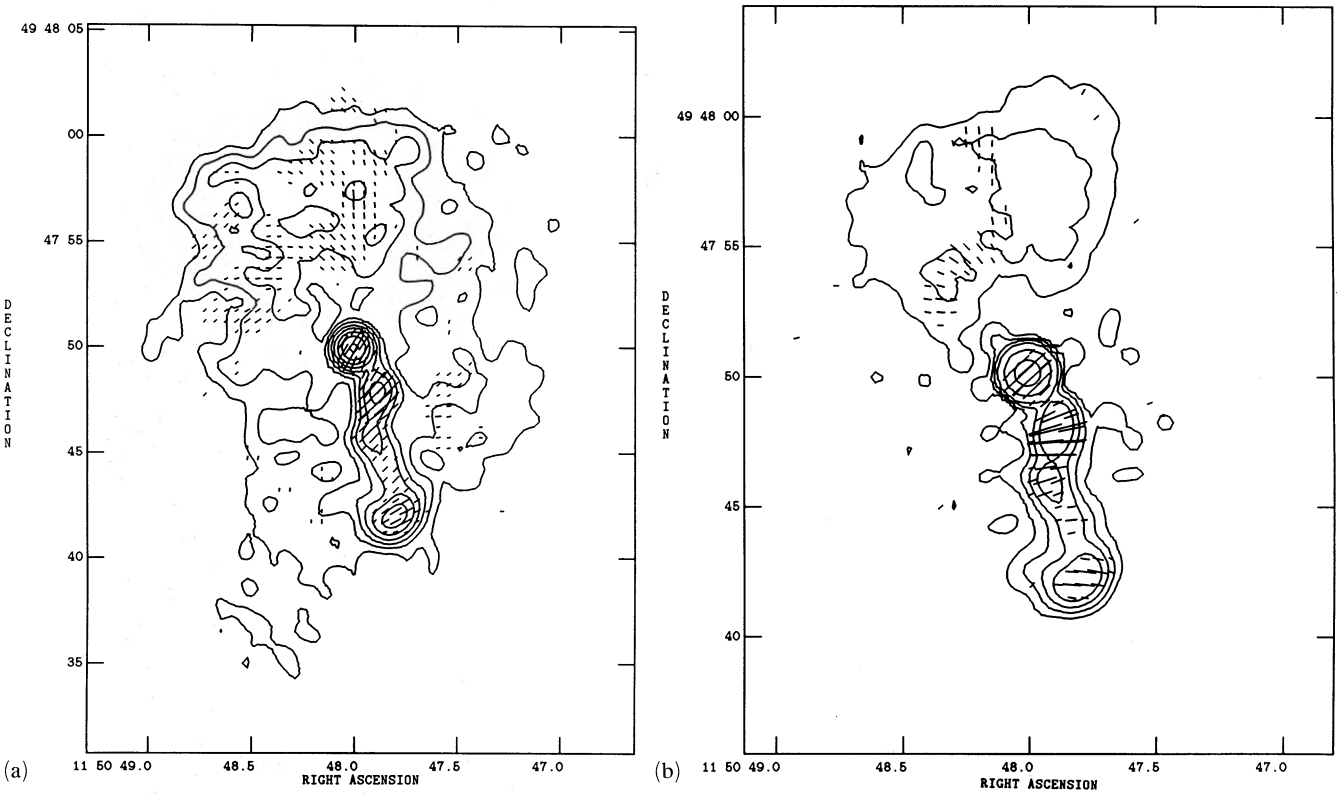

Figure 2. (a) VLA 1.6-GHz map of 1150+497. The restoring beam is 1.0 arcsec and contour levels are $5 \times (0.25, 0.5, 1, 2, 4, 8, \ldots)$ mJy beam^{-1} and peak brightness is 368 mJy beam^{-1}. One arcsec represents a polarized intensity of 5.33 mJy beam^{-1}. (b) VLA 5-GHz map with a restoring beam of 1 arcsec. The contour levels are $5 \times (0.25, 0.5, 1, 2, 4, 8, \ldots)$ mJy beam^{-1} and peak brightness is 302 mJy beam^{-1}. One arcsec represents a polarized intensity of 2.67 mJy beam^{-1}.

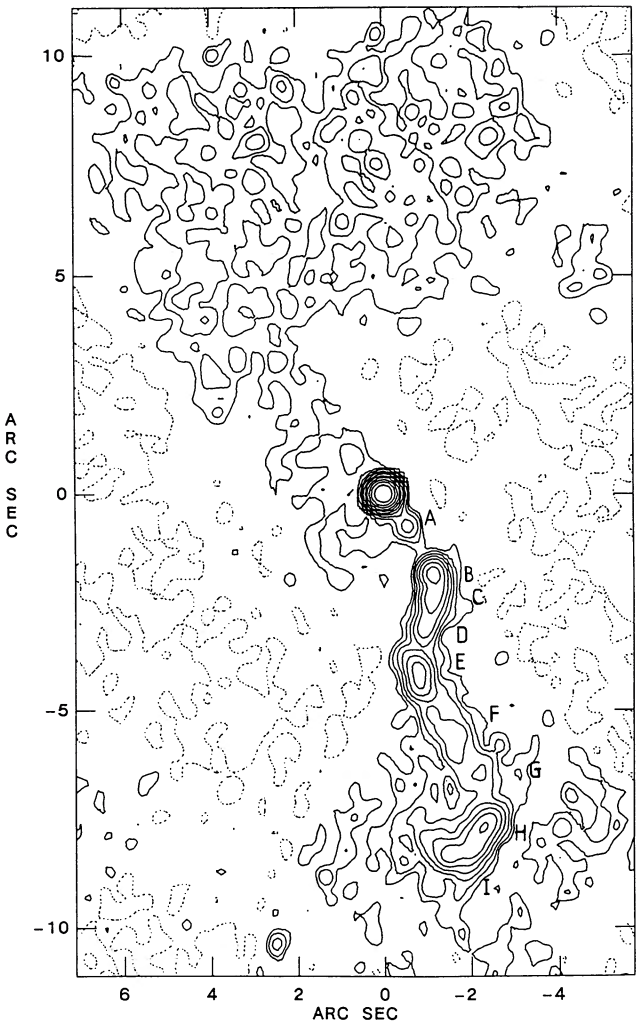

Figure 3. VLA 5-GHz map of 1150+497. The restoring beam is 0.35 arcsec and the contour levels are $0.5\times(0.25, 0.5, 1, 2, 4, 8,\ldots)$ mJy beam^{-1}. The peak brightness is 324 mJy beam^{-1}.

dominated quasars (Saikia & Shastri 1984). Along the jet, the degree of polarization is high, about 15 per cent, with the ***B***-vector following accurately the path of the jet except at the end of the jet where it is almost perpendicular to the jet direction (Fig. 2a). At knots E and F there appears to be a transverse offset between the maxima of total and polarized intensity (Fig. 5). A similar effect is seen in 0800+608 (Jackson *et al.* 1990) and has been interpreted in terms of a jet consisting of twisted flux tubes (Königl & Choudhuri 1985). In the northern lobe the degree of polarization is also about 15 per cent.

Fig. 6 shows a map of the Faraday rotation measure RM derived by least-squares fits to polarization position angle χ versus λ^2 for the 1.4-, 1.5-, 1.6- and 4.9-GHz maps. Only points where the noise error in χ was less than 10° are shown. There is some variation of RM along the jet and an increase from 15 rad m^{-2} at the core to 25 rad m^{-2} at knot F. The RM pattern does not appear to be related to the pattern of knots in the jet but has a smooth gradient along the jet. The RM values are less certain in the northern lobe but are mostly in the range 8–15 rad m^{-2}.

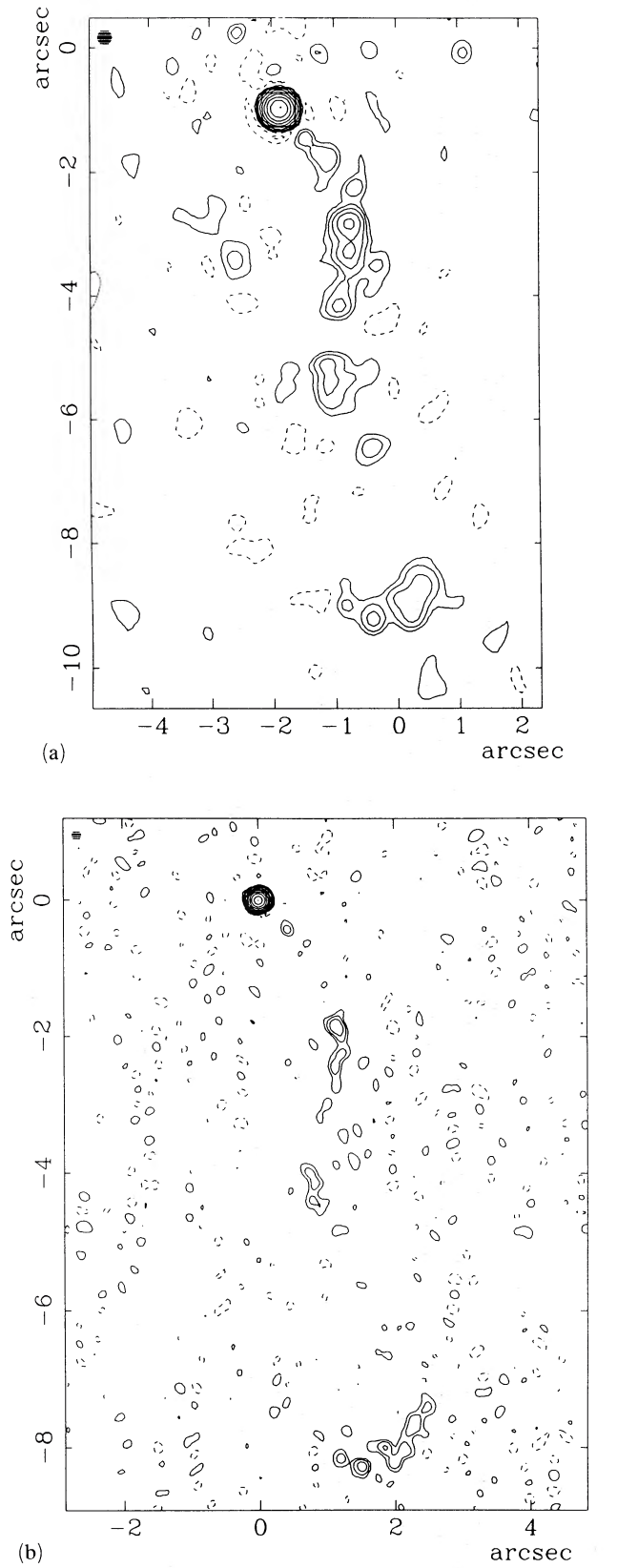

Figure 4. (a) MERLIN 1.6-GHz map of 1150+497. The restoring beam is 0.25 arcsec and the contour levels are 0.2, 0.4, 0.8, 1.6, 3.2,... per cent of the peak brightness which is 498 mJy beam^{-1}. (b) MERLIN 5-GHz map. The restoring beam is 150 mas and contour levels are at 0.2, 0.4, 0.8, 1.6, 3.2,...per cent of the peak brightness which is 420 mJy beam^{-1}.

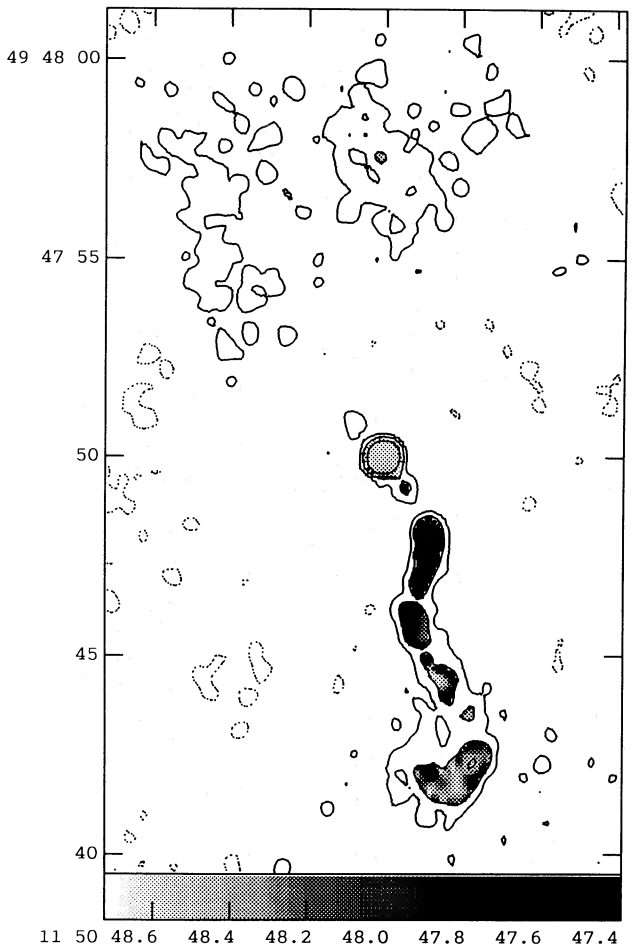

Figure 5. A grey-scale representation of the distribution of percentage polarization superimposed on the VLA 5-GHz map. The scale is from 0 to 20 per cent. The restoring beam of the map is 0.35 arcsec.

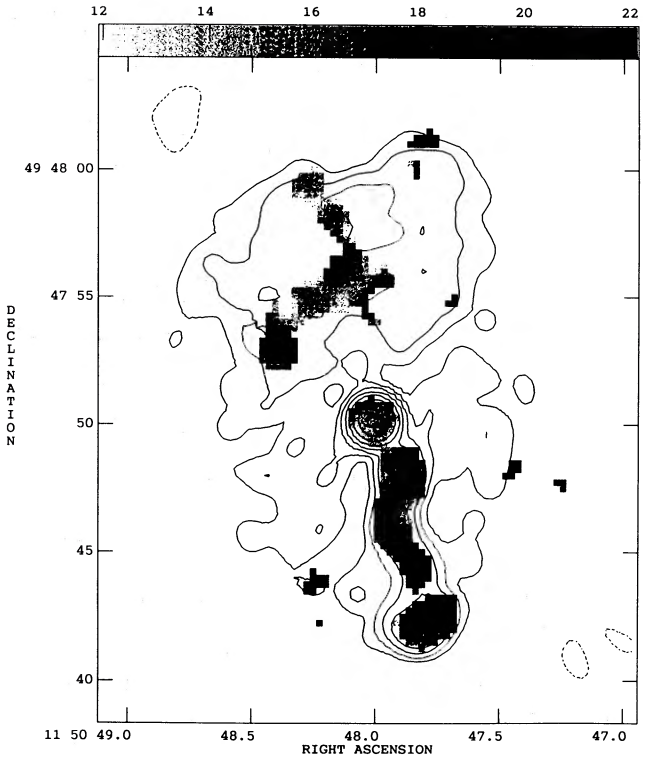

Figure 6. A grey-scale representation of the distribution of Faraday rotation (in units of rad m^{-2}) superimposed on the low-resolution VLA map at 1.5 GHz. The map restoring beam is 1 arcsec.

Between 5 and 15 GHz, the RM increases to -163 rad m^{-2}. Holmes & Saikia (private communication) have shown that bright cores often show large rotations in polarization position angles at high frequency and suggest that this occurs because the high-frequency emission comes from deeper within an optically thick core with large Faraday depths.

The rotation measure RM gives the average Faraday depth $\phi = \int nB_z\, dl$, where n is the thermal electron density and B_z is the magnetic flux density along the line-of-sight. If ϕ is expressed in units of cm^{-3} μG pc then $RM = 0.81\langle\phi\rangle$. Variations in ϕ, either in an irregular Faraday screen or within the source, lead to depolarization with increasing wavelength. Since we find no significant depolarization between 6 and 20 cm in the jet, we may set an upper limit to the standard deviation of ϕ, $\Delta < 13.3$ cm^{-3} μG pc. The northern lobe shows slight repolarization between 20 and 6 cm, which may suggest a slightly higher value of $\Delta = 15$ cm^{-3} μG pc (see Garrington, Conway & Leahy 1991).

The integrated degree of polarization remains constant at 3–4 per cent from 6–73 cm (Conway *et al.* 1972). This implies that the northern lobe and the halo, which are the dominant components at $\lambda > 20$ cm, have $\Delta \lesssim 3$ cm^{-3} μG pc. The value of Δ for 1150+497 is usually low for a quasar of its angular size and redshift (Strom 1973; Garrington & Conway 1991).

5 DISCUSSION

At some level all extragalactic radio sources consist of a core, a jet (which may be one- or two-sided), hotspots and lobes. The chief difference between them is in the relative prominence of these components. In lobe-dominated quasars, the jet typically accounts for between 1–10 per cent of the total flux density, and the hotspots account for 10–50 per cent. 1150+497 is unusual in that the jet accounts for 25 per cent of the total source flux at 20 cm, while any hotspot emission accounts for only 1 per cent.

Why is the jet so prominent in 1150+497? We consider two models: (1) the jet brightness is enhanced because the jet loses more of its kinetic energy along its length rather than in a terminal hotspot (Swarup *et al.* 1982) and (2) the jet dominance is due to Doppler beaming.

5.1 A disrupting jet?

Jets can be disrupted for two reasons; if they collide with dense clumps of material in the surrounding medium, or if they are hydrodynamically unstable.

We consider first collisions with dense clumps: the jet can be disrupted if the pressure in the clumps is comparable to the jet ram pressure. A lower limit on the jet ram pressure is

given by the internal energy of the knots in the jet. Using the traditional equipartition arguments (Miley 1980) we estimate the internal energy of the brightest knot as 1×10^{-10} N m^{-2}. An upper limit on the density of the clumps is given by assuming that they are responsible for the observed Faraday rotation variations of order $\Delta\phi \simeq 10$ cm^{-3} μG pc along the jet. For an individual clump the Faraday depth is

$$\phi_c = n_c B_c d_c, \quad (1)$$

where n_c, B_c and d_c are the density, average line-of-sight magnetic field strength and size. The size must be larger than the jet diameter but smaller than the distance between bends, say 10 kpc. Hence $n_c \sim 10^{-3}\,(B/\mu\mathrm{G})^{-1}$ cm^{-3}. For temperatures in the range 10^4–10^7 K the gas pressure is 10^{-16}–10^{-13} N m^{-2}. The jet would therefore be hardly affected by the clouds.

We now consider hydrodynamical instabilities. Numerical simulations of the propagation of jets through a uniform medium (Norman *et al.* 1982) show that jets which have comparable densities to their surroundings are more susceptible to Kelvin–Helmholtz instabilities than lighter jets. 'Heavy' jets do not produce large backflowing cocoons and have been proposed for other 'naked-jet' sources such as 0800+608 (Shone & Browne 1986). The low Faraday dispersion of 1150+497 suggests that this density balance arises because the environment is usually sparse rather than because the jet is unusually dense.

Again, we may use the Faraday rotation to estimate the density of a surrounding halo of gas containing a tangled magnetic field. Using

$$\Delta = n_x B_x (Ld)^{1/2}, \quad (2)$$

where L is the path length through the medium which must be comparable to the jet length, and d is the tangling scale of the magnetic field, say 10 kpc, we estimate the density as $n_x \sim 5 \times 10^{-4}\,(B/\mu\mathrm{G})^{-1}$.

The instabilities grow as wiggles in the jet and simulations of the response of jets to small perturbations in direction near the core (Norman & Hardee 1988) give a resonant wavelength λ of

$$\lambda \simeq \frac{2M}{m(1+\eta^{1/2})}\, r_j, \quad (3)$$

where r_j is the jet radius, η is the ratio of jet to ambient density and M is the jet Mach number. For $\eta \sim 1$ and $m = 1$ (fundamental mode) we expect a resonant wavelength of $\lambda/r_j \sim M$. Tracing the jet wiggle from the VLA 6-cm map we obtain $\lambda/r_j \sim M \sim 10$. If the jet is in pressure equilibrium with a surrounding halo of gas at 10^7 K, then this implies a jet velocity $\sim 10^4$ km s^{-1}.

The numerical simulations show that such jets have a characteristic disruption length of a few times λ. The jet ends not in a hotspot but in a lobe created by the large oscillations in jet direction. This may be identified with the final section of the jet and the surrounding lobe in 1150+497.

5.2 Relativistic beaming

If the jet is at a small angle θ to the line-of-sight and has a relativistic bulk velocity, Doppler beaming may boost its flux density above that of lobes and hotspots. Projection effects would account naturally for the appearance of the halo as two overlapping lobes and would amplify small intrinsic bends in the jet. Doppler beaming would naturally account for the lack of a counterjet.

The jet velocity required to boost its flux density by a factor of 10 relative to the hotspot depends on the angle, θ. A consistent set of parameters would be $\theta \sim 12°$, jet speed $\beta_j = 0.9$ and hotspot speed $\beta_h < 0.6$. (We need not identify β_h as the lobe advance speed which may be somewhat slower.) Using these parameters, the jet to counter-jet brightness ratio would be of order 1000:1 compared to the observed lower limit of 50:1 from the VLA 6-cm map. The ratio of the brightness of the approaching and receding hotspots would be about 10:1, similar to the lower limit measured from the MERLIN 6-cm map.

Bends in the jet may give rise to substantial variations in brightness along the jet. The observed contrast in the jet would require $\beta_j \sim 0.95$ if the bends are comparable to θ. However, one might then expect still larger apparent bends in the jet, unless by chance the bends are largely confined to a plane containing the line-of-sight.

6 CONCLUSIONS

New maps of the quasar 1150+497 have revealed a bright jet which contains compact knots with high surface brightness and sharp bends. The middle, weaker part of the jet appears to be well collimated. The final section of the jet is very distorted and does not have a prominent hotspot. The magnetic field is mainly parallel to the jet direction except at the final knot. There is little variation of rotation measure or evidence of depolarization throughout the whole source.

Hydrodynamical models suggest that the jet in 1150+497 is unstable and disrupts catastrophically before forming a hotspot. This requires that the densities of the jet and surrounding medium are comparable: the low Faraday dispersion suggests that this is because the surrounding medium is unusually sparse. This model does not easily account for the very compact knots, the sharp bends or the lack of a counterjet on the opposite side of the source. Relativistic beaming may boost the flux density of the jet relative to the lobe and hotspots, and hide the counterjet if it is at a small angle to the line-of-sight. In this model the bright knots correspond to those parts of the jet with velocities close to the line-of-sight. However, this model requires rather contrived fine tuning to account for all the observed features.

We are currently engaged in detailed observations of a sample of sources with bright jets but no hotspots to investigate which features are common in this class of sources. This should help to determine whether these are disrupting jets or extreme cases of Doppler beaming.

ACKNOWLEDGMENTS

We are grateful to Drs D. J. Saikia and I. W. A. Browne for granting us access to their unpublished data. CEA acknowledges a Royal Society Fellowship at Jodrell Bank. He is also grateful to Professors F. G. Smith and R. D. Davies, the Director, NRAL for hospitality and encouragement. STG was supported by a SERC fellowship.

REFERENCES

Baars, J. W. M., Genzel, R., Pauliny-Toth, I. I. K. & Witzel, A., 1977. *Astr. Astrophys.*, **61,** 99.

Blandford, R. D. & Rees, M. J., 1974. *Mon. Not. R. astr. Soc.,* **169,** 395.

Conway, R. G., Gilbert, J. A., Kronberg, P. P. & Strom, R. G., 1972. *Mon. Not. R. astr. Soc.,* **157,** 443.

Cornwell, T. J. & Wilkinson, P. N., 1981. *Mon. Not. R. astr. Soc.,* **196,** 1067.

Davis, R. J., Muxlow, T. W. B. & Conway, R. G., 1985. *Nature,* **318,** 343.

Garrington, S. T. & Conway, R. G., 1991. *Mon. Not. R. astr. Soc.,* **250,** 198.

Garrington, S. T., Conway, R. G. & Leahy, J. P., 1991. *Mon. Not. R. astr. Soc.,* **250,** 171.

Jackson, N., Browne, I. W. A., Shone, D. L. & Lind, K. R., 1990. *Mon. Not. R. astr. Soc.,* **244,** 750.

Königl, A. & Choudhuri, A. R., 1985. *Astrophys. J.,* **289,** 173.

Kühr, H., Witzel, A., Pauliny-Toth, I. I. K. & Nauber, U., 1981. *Astr. Astrophys. Suppl.,* **45,** 367.

Linfield, R., 1983. *Astrophys. J.,* **275,** 461.

Miley, G. K., 1980. *Ann. Rev. Astr. Astrophys.,* **18,** 165.

Norman, M. L. & Hardee, P. E., 1988. *Astrophys. J.,* **334,** 80.

Norman, M. L., Smarr, L., Winkler, K. H. A. & Smith, M. D., 1982. *Astr. Astrophys.,* **113,** 285.

Owen, F. N. & Puschell, J. J., 1984. *Astr. J.,* **89,** 932.

Owen, F. N., Hardee, P. E. & Cornwell, T. J., 1989. *Astrophys. J.,* **340,** 698.

Perley, R. A., 1981. In: *Optical Jets in Galaxies,* p. 77, eds Battrick, B. & Mort, J., European Space Agency: Paris.

Perley, R. A., 1982. *Astr. J.,* **87,** 859.

Saikia, D. J. & Shastri, P., 1984. *Mon. Not. R. astr. Soc.,* **211,** 47.

Saikia, D. J., Shastri, P., Cornwell, T. J. & Banhatti, D. G., 1983. *Mon. Not. R. astr. Soc.,* **203,** 53P.

Scheuer, P. A. G., 1974. *Mon. Not. R. astr. Soc.,* **166,** 513.

Shone, D. L. & Browne, I. W. A., 1986. *Mon. Not. R. astr. Soc.,* **222,** 365.

Strom, R. G., 1973. *Astr. Astrophys.,* **25,** 303.

Swarup, G., Sinha, R. P. & Saikia, D. J., 1982. *Mon. Not. R. astr. Soc.,* **201,** 393.